

## Article

# Effects of Gd/Nd Ratio and Aging Treatment on Wear Behavior of Mg-Nd-Gd-Sr-Zn-Zr Alloys

Ruotian Wang<sup>1,2</sup>, Rongxiang Wang<sup>3</sup> and Yongqiang Jia<sup>3,\*</sup><sup>1</sup> Nanjing University of Aeronautics and Astronautics, Nanjing 211106, China; ruotianw@outlook.com<sup>2</sup> Yongli Filament & Bristles Co., Limited, Nanjing 210016, China<sup>3</sup> School of Materials Science and Engineering, Nanjing Institute of Technology, Nanjing 211167, China; rongxiangwang2023@126.com

\* Correspondence: jiaoyongqiang93@163.com

**Abstract:** The Mg-(4-x)Nd-xGd-0.3Sr-0.2Zn-0.4Zr (x = 0, 1, 2, and 3 wt%, Gd/Nd = 0, 1/3, 1, and 3) alloys were hot extruded and then aged (T5). The friction and wear properties of the as-extruded and as-aged alloys were studied using a ball-on-disk wear testing machine and a scanning electron microscope to reveal the impacts of the Gd/Nd ratio and aging treatment. The results show that the friction coefficient of the as-extruded alloys increases first and then decreases with increasing Gd/Nd ratio. After aging, the friction coefficient of the alloys decreases slightly. The Gd/Nd ratio has no significant effect on the wear rate of the as-extruded alloys, and the wear rate decreases first and then increases with the increase in the Gd/Nd ratio for the as-aged alloys. The T5 alloy with a Gd/Nd ratio of 1/3 has the best wear resistance. The wear mechanisms of alloys mainly include abrasive wear, oxidation wear, and delamination wear.

**Keywords:** magnesium alloy; friction coefficient; wear rate; wear mechanism



**Citation:** Wang, R.; Wang, R.; Jia, Y. Effects of Gd/Nd Ratio and Aging Treatment on Wear Behavior of Mg-Nd-Gd-Sr-Zn-Zr Alloys. *Coatings* **2024**, *14*, 7. <https://doi.org/10.3390/coatings14010007>

Academic Editor: Roberto Montanari

Received: 29 November 2023

Revised: 15 December 2023

Accepted: 18 December 2023

Published: 20 December 2023



**Copyright:** © 2023 by the authors. Licensee MDPI, Basel, Switzerland. This article is an open access article distributed under the terms and conditions of the Creative Commons Attribution (CC BY) license (<https://creativecommons.org/licenses/by/4.0/>).

## 1. Introduction

In recent years, magnesium (Mg) alloys have attracted wide attention due to their desirable advantages, such as low density, high specific strength, high specific stiffness, and good casting performance [1–5]. As a substitute material for traditional structural metal materials, Mg alloys have been applied in many fields, such as the automobile industry and aerospace industry, for better system performance and energy efficiency, showing good industrial application prospects [6–8]. In automobile and aerospace fields, the friction and wear properties of engine systems or equipment power components, such as bearings and gears, are important indicators because wear can easily cause degradation or failure of product properties, thus increasing safety risks and economic losses [9–11]. However, the problem of poor wear resistance of Mg alloys still exists at present, which limits their further application in related fields.

The composition and processing technology will obviously affect the microstructure of Mg alloys and then affect the tribological properties. Generally, the common methods to improve the friction and wear properties of Mg alloys are alloying and plastic deformation [12–15]. As a metal “nutrient”, rare earth (RE) elements alloying can improve the mechanical properties of Mg alloys. The RE elements commonly added in Mg alloys include Gd, Nd, Y, La, Ce, Yb, etc. [16,17]. The effects of RE elements on the friction and wear properties of Mg alloys have not been fully studied, and most reports show that the addition of RE elements is beneficial to wear resistance due to the refined structure and the formation of a stable second phase [18–20]. In addition, heat treatment has an important effect on the tribological properties of Mg alloys [21–23]. It was found that the wear resistance of the AZ91-1.0%Pr alloy under the T6 condition was much better compared with that under the as-cast and T4-treated conditions, which was mainly due to large amounts of fine precipitates in the grains and grain boundaries [21]. The wear resistance of the

alloy T6-treated AZ91/3.0WC increased by about 63% due to the presence of Mg<sub>17</sub>Al<sub>12</sub> precipitates [22]. However, T6 treatment on as-cast Mg-10Gd-3Y-0.4Zr increased the wear rate because the eutectic compound, which could resist wear, almost disappeared after the T6 treatment [23]. Nevertheless, few studies on post-extrusion aging (T5) are available on the friction and wear properties of Mg alloys.

In our previous work, Microstructure, tensile properties, and corrosion behavior of the as-cast, T6-treated, and as-extruded Mg-(4-x)Nd-xGd-0.3Sr-0.2Zn-0.4Zr alloys have been studied, and the alloys exhibit good tensile and anticorrosion properties [24,25]. In this present work, the effects of the Gd/Nd composition ratio and T5 treatment on the friction and wear properties of the as-extruded Mg-(4-x)Nd-xGd-0.3Sr-0.2Zn-0.4Zr alloys were investigated, its structural evolution and wear mechanism were also discussed in detail.

## 2. Materials and Methods

### 2.1. Alloy Preparation

Mg-(4-x)Nd-xGd-0.3Sr-0.2Zn-0.4Zr (x = 0, 1, 2 and 3 wt%, denoted as Alloy 0, 1, 2, and 3) alloys with different Gd/Nd ratios (Gd/Nd = 0, 1/3, 1, and 3) were prepared using a gravity casting process. The raw materials used in the experiment are pure Mg, pure Zn, and Mg-30%Nd, Mg-30%Gd, Mg-25%Sr, and Mg-30%Zr master alloys. Melting was carried out in a resistance crucible furnace protected with mixed gas (CO<sub>2</sub> + SF<sub>6</sub>). When the raw materials were completely melted, they were stirred for 5 min and then kept for 15–20 min to cool to 720 °C. The molten liquid was then cast into a preheated die and cooled in water. The four alloys were heated to 540 °C and held for 12 h, then quenched with water to obtain homogeneous microstructures. After removing the surface oxide layer using a lathe, the solution-treated ingots were hot extruded at 330 °C with an extrusion ratio of 9 and extrusion speed of 2 mm/s. The specimens under the as-extruded condition were denoted as E. Part of the as-extruded rods were aged at 200 °C for 12 h, which was denoted as T5.

### 2.2. Testing Methods

The specimens under as-extruded and as-aged states were roughly ground with W50 sandpaper first and then finely ground with W 20 and W10 sandpaper, respectively. Finally, the specimens were polished using a polishing machine and etched using a picric acid solution. An optical microscope (OM, GX51, Olympus, Tokyo, Japan), a scanning electron microscope (SEM, JSM-6360LV, JEOL, Tokyo, Japan), and an energy dispersive spectrometer (EDS, GENESIS 2000XM60, West Orange, NJ, USA) were used to observe the microstructure and element distribution of alloys under both as-extruded and as-aged conditions. Microhardness of the alloys was carried out on a Vickers hardness tester (FM-700, Shanghai, China) under a load of 500 gf and a dwell time of 10 s.

Before wear experiments, specimens were ground and polished to make their surfaces free from obvious scratches. A MFT-3000 ball-disc wear machine (RETC, Fremont, CA, USA) was used in this experiment. The schematic diagram of the friction and wear experiment is shown in Figure 1. During the whole experiment, the sliding speed was 25 mm/s, the sliding time was 60 min, and the applied load was 100 N. After the experiment, the abrasive debris on the surfaces of the samples was glued with conductive adhesive, and the samples were placed in a beaker filled with alcohol, cleaned with ultrasonic for 3 min, and then blow-dried. SEM equipped with EDS was used to observe the wear morphologies and debris of the samples, and the distribution of elements of wear products and debris was analyzed.

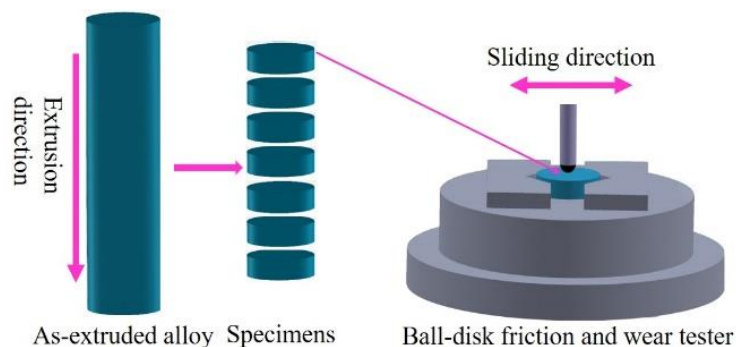


**Figure 1.** Schematic diagram of friction and wear experiment.

### 3. Results

#### 3.1. Microstructure and Microhardness

Figure 2 shows the microstructure perpendicular to the extrusion direction of the alloys with different Gd/Nd ratios. The microstructures of both as-extruded and as-aged alloys are mostly composed of bright, fine equiaxed  $\alpha$ -Mg recrystallized grains, grey secondary phase grains at matrix grain boundaries, and tiny precipitates. Some large grains can be observed in E-alloy 0, which are free from dynamic recrystallization [25]. With the increase in Gd/Nd ratio, the microstructure of the as-extruded alloys becomes more uniform with less long elongated grains and secondary phase, and the grain size shows an invisible difference, which is in the range of 3–6  $\mu\text{m}$ . Compared with the as-extruded alloys, the grain size in T5-alloy 0 reduces due to static recrystallization, and the grain sizes of the T5-alloy 2 and T5-alloy 3 become coarser than those of the as-extruded alloys.

Figure 3 shows the SEM images of E-alloy 0 and E-alloy 3 with their corresponding element distribution maps. According to the binary phase diagrams of Mg-Gd and Mg-Nd, the ultimate solid solubility of Gd and Nd in Mg are 23.49 wt% and 3.6 wt%, respectively [26]. It is clear that much Nd is aggregated in the eutectic phase of the E-alloy 0, which was confirmed as Mg<sub>41</sub>Nd<sub>5</sub> [27]. As for the E-alloy 3, most of the alloying elements dissolve into the matrix and distribute more homogeneously.

Figure 4 presents the SEM micrographs of E-alloy 1 and T5-alloy 1, and the EDS results of the marked regions are listed in Table 1. It is much clearer to observe the secondary phase grains and tiny precipitates at high magnification. The secondary phase grain in E-alloy 1 (region 1) is composed of Mg, Nd, Gd, and Zn, but after T5 treatment, the content of Nd, Gd, and Zn decreases, and 1.64% Sr is present, which is shown in the secondary phase grain in T5-alloy 1 (region 4). As for the E-alloy 1, region 2 shows that tiny precipitates are composed of Mg, Nd, Gd, Sr, Zn, and Zr, and the contents of Nd, Gd, and Zn are lower than the values of those in the secondary phase grain. Region 3 shows that  $\alpha$ -Mg is composed of Mg, Gd, Zn, and Zr.

The microhardness of the alloys with different Gd/Nd ratios under as-extruded and as-aged conditions is presented in Figure 5. For the alloys 0, 1, and 2, the microhardness values changed very little and can be neglected as increases in the Gd/Nd ratio. But when the Gd/Nd ratio is 3, its microhardness value is 57.5 HV, which decreased by about 10% compared with that of the Alloy 0. After the T5 aging treatment, the microhardness of alloys with several Gd/Nd ratios shows an 8.4–13.6% improvement, and among these, the microhardness of the Alloy 1 sample increased from 62.5 HV to 69.0 HV. With the increases in the Gd/Nd ratio, the microhardness of T5 aging samples displayed a similar trend as the as-extruded samples.

#### 3.2. Friction and Wear Properties

Figure 6 shows the representative friction coefficient curves and average values of the alloys under as-extruded and as-aged conditions. Generally, the friction coefficient fluctuates greatly at the beginning stage of dry sliding (0–400 s), which is in the run-in stage. Then, the friction coefficients have slight fluctuations when prolonging the experimental

time, which may have resulted from the metal oxide layer formed between the grinding ball and the sample surface, as well as the continuously generated wear debris at the interface [28]. The representative friction coefficient curves of the alloys with different Gd/Nd ratios under both conditions present the same tendency. The friction coefficient value of the alloys is between 0.335 and 0.351, showing only a slight difference. Since the friction coefficient difference is less than 5%, the effect of the Gd/Nd ratio on the friction coefficient of the alloys under both conditions is negligible, especially for the as-aged alloys. Nevertheless, compared with the as-extruded alloys, the as-aged alloys present a slightly lower friction coefficient which is probably due to the higher microhardness.

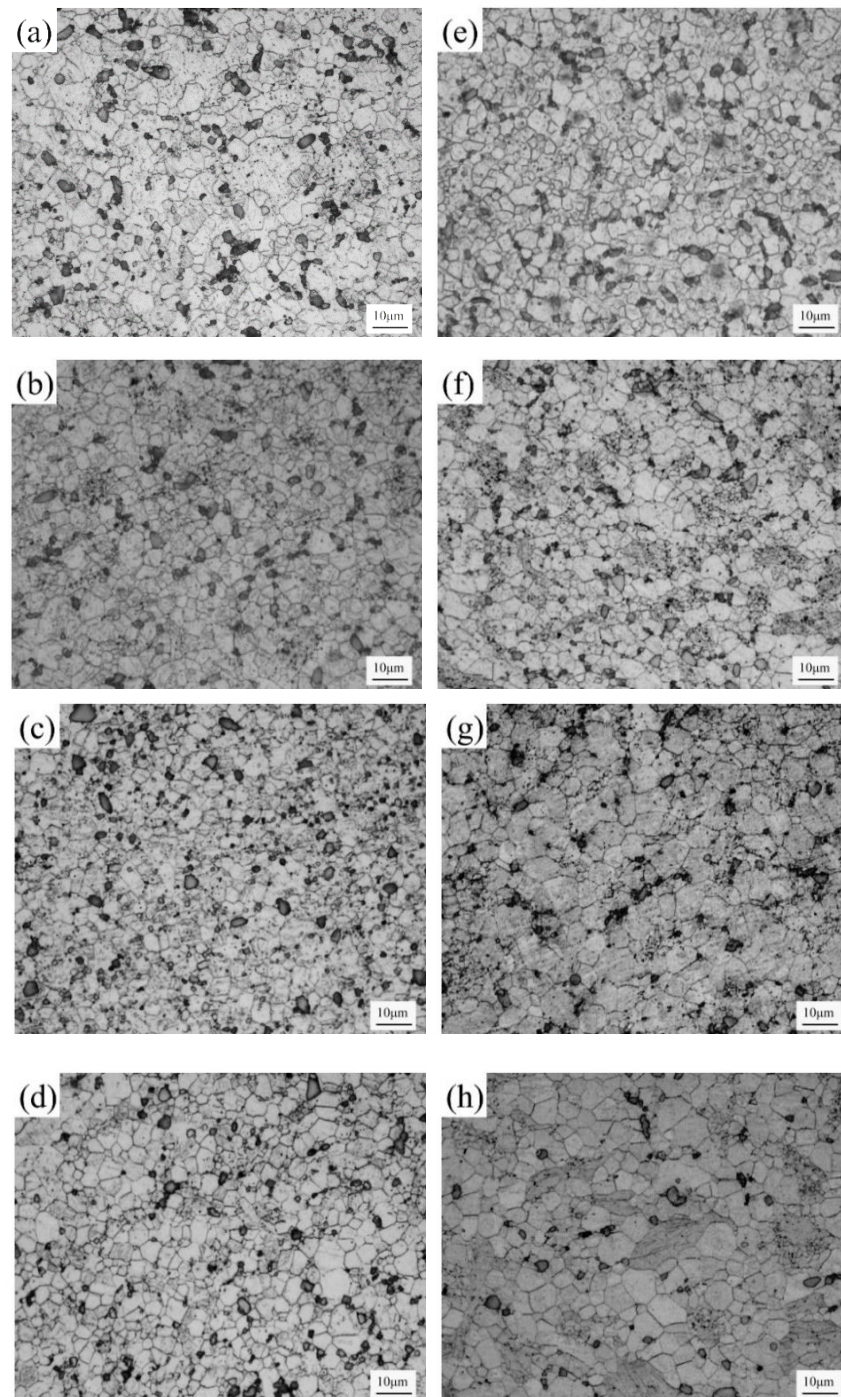


**Figure 2.** Optical micrographs of Mg-Nd-Gd-Sr-Zn-Zr alloys (a) E-alloy 0, (b) E-alloy 1, (c) E-alloy 2, (d) E-alloy 3, (e) T5-alloy 0, (f) T5-alloy 1, (g) T5-alloy 2, (h) T5-alloy 3.

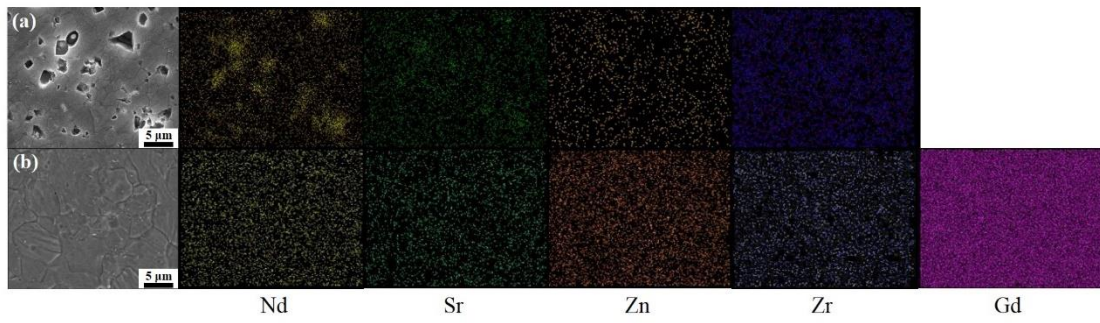


Figure 3. SEM images and alloying elements distribution maps of the E-alloy 0 (a) and E-alloy 3 (b).

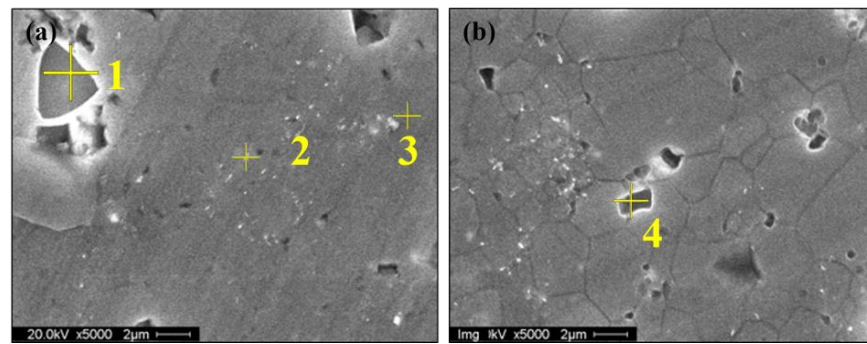


Figure 4. SEM images of alloy 1; (a) E-alloy 1, (b) T5-alloy 1.

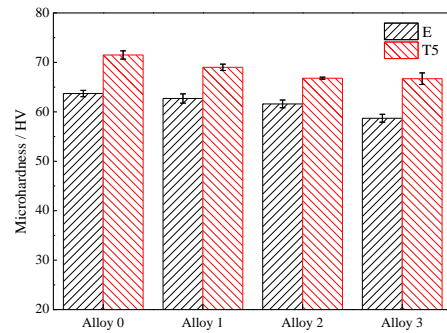
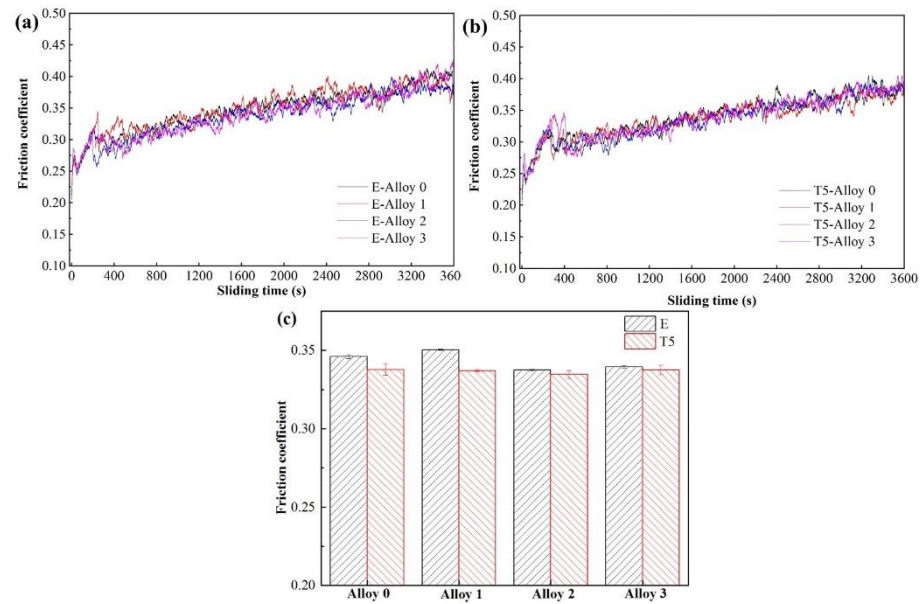


Figure 5. Microhardness of the as-extruded and as-aged alloys.

Table 1. Compositions of the marked regions in Figure 4.

Element Content/wt.%	1	2	3	4
Mg	67.35	93.31	93.05	83.69
Nd	27.76	1.95	3.42	11.99
Gd	2.76	1.45	1.73	1.66
Sr	/	1.03	/	1.64
Zn	1.65	1.05	0.87	1.02
Zr	/	1.2	0.94	/

Figure 7 shows the mass wear rates of the alloys at as-extruded and as-aged states after 60 min dry sliding. It can be seen that the mass wear rate difference of the as-extruded alloys with different Gd/Nd ratios is very slight (<3.5%). After the T5 treatment, with the increase in Gd/Nd ratio, the mass wear rate of alloys first decreases and then increases, among them the mass wear rate of the T5-alloy 1 is the lowest. It is worth noting that the mass wear rate of T5-alloy 0 is higher than that of the E-alloy 0, but the result for alloy 1 is contrary, indicating the complex effect of the T5 treatment on the wear rate of the alloys. The maximum mass wear rate is T5-alloy 0, and the minimum of it is T5-alloy 1.



**Figure 6.** Representative friction coefficient curves of (a) E alloys and (b) T5 alloys and (c) friction coefficient average values of the alloys.

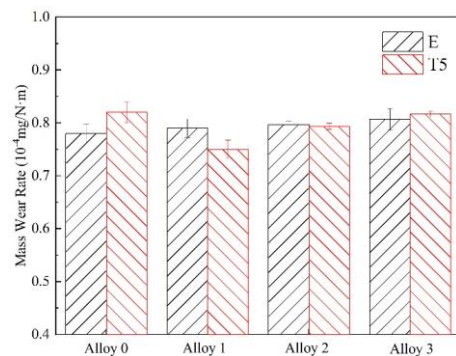


**Figure 7.** Mass wear rates of the alloys after 60 min dry sliding.

The wear surfaces of the alloys were observed using SEM, as shown in Figure 8. The compositions of some regions marked in Figure 8 are listed in Table 2. It can be seen from Figure 8 that there are many smooth furrows parallel to the sliding direction on the wear surfaces, showing typical abrasive wear [29,30]. Some hard particles embedded into the furrows can be visible in Figure 8a,d,f, which are responsible for the abrasive wear. Specially, the fine particle circled in Figure 8d is probably the secondary phase because it is composed of more alloying elements than the matrix, as shown in Table 2, which is involved in the abrasive wear. Moreover, some peeling pits are also observed in the wear morphologies (red circle areas), indicating the existence of delamination wear [31], which results in the abrasive debris shown in Figure 9, and the abrasive debris is composed of Mg, Nd, Gd, Sr, Zn, and O. In addition, rough areas can also be found from the wear morphologies. As shown in Figure 8c, The EDS analysis of the region 1 area in Table 2 reveals the existence of oxygen element, which means oxidation wear. Therefore, for the E-alloys and T5-alloys, the wear mechanism includes abrasive wear, oxidation wear, and delamination wear. It is worth mentioning that the more abrasive the particles, the deeper the furrows, and fewer peeling marks are shown on the T5-Alloy 1 surface, indicating that its main wear mechanisms are abrasive wear and oxidation wear.

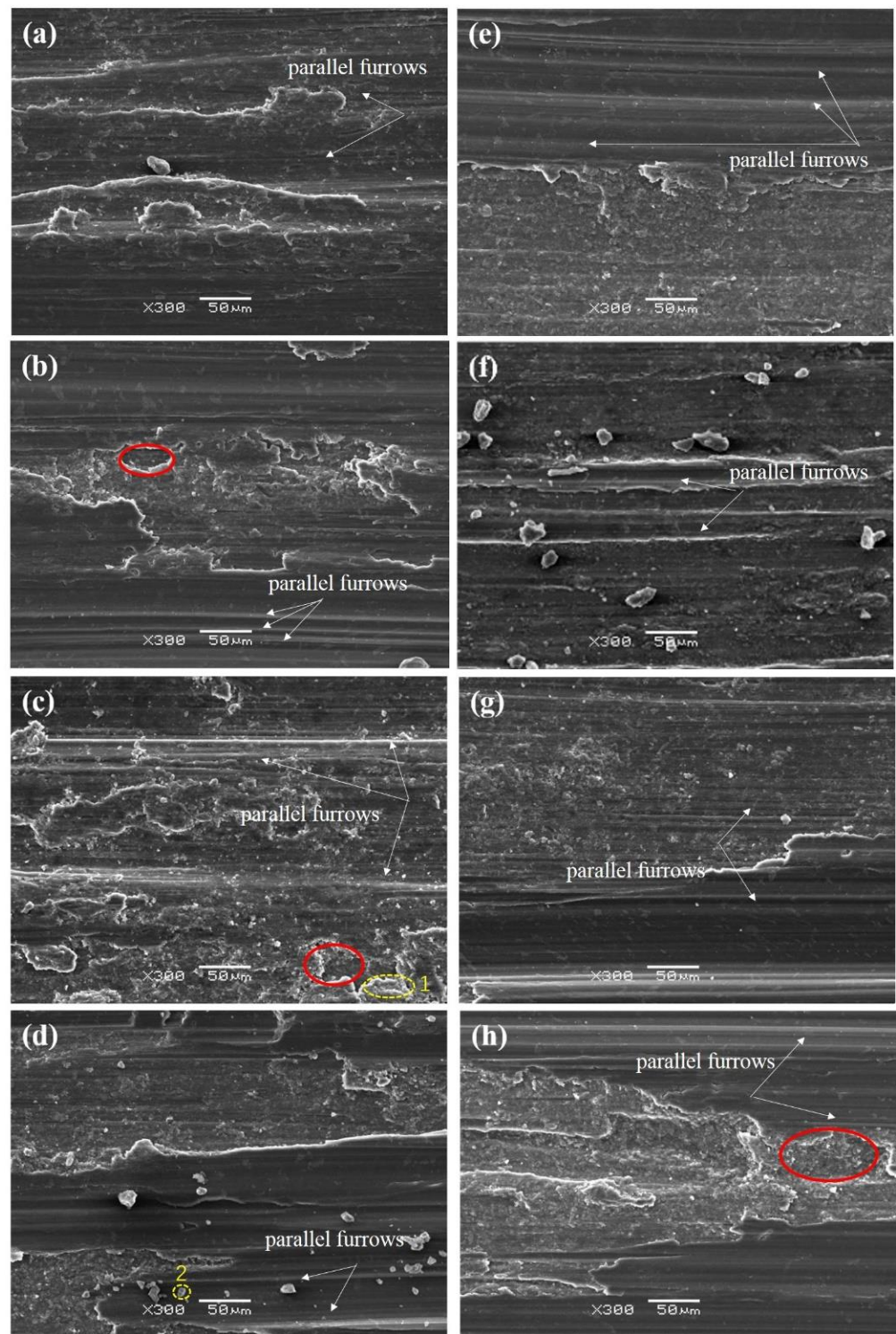


**Figure 8.** SEM images of wear surfaces of the as-extruded (a–d) and as-aged (e–h) alloys. (a) E-Alloy 0; (b) E-Alloy 1; (c) E-Alloy 2; (d) E-Alloy 3; (e) T5-Alloy 0; (f) T5-Alloy 1; (g) T5-Alloy 2; (h) T5-Alloy 3. The arrows are parallel furrows and the red circles are the peeling marks. The EDS results of yellow circles are shown in Table 2.

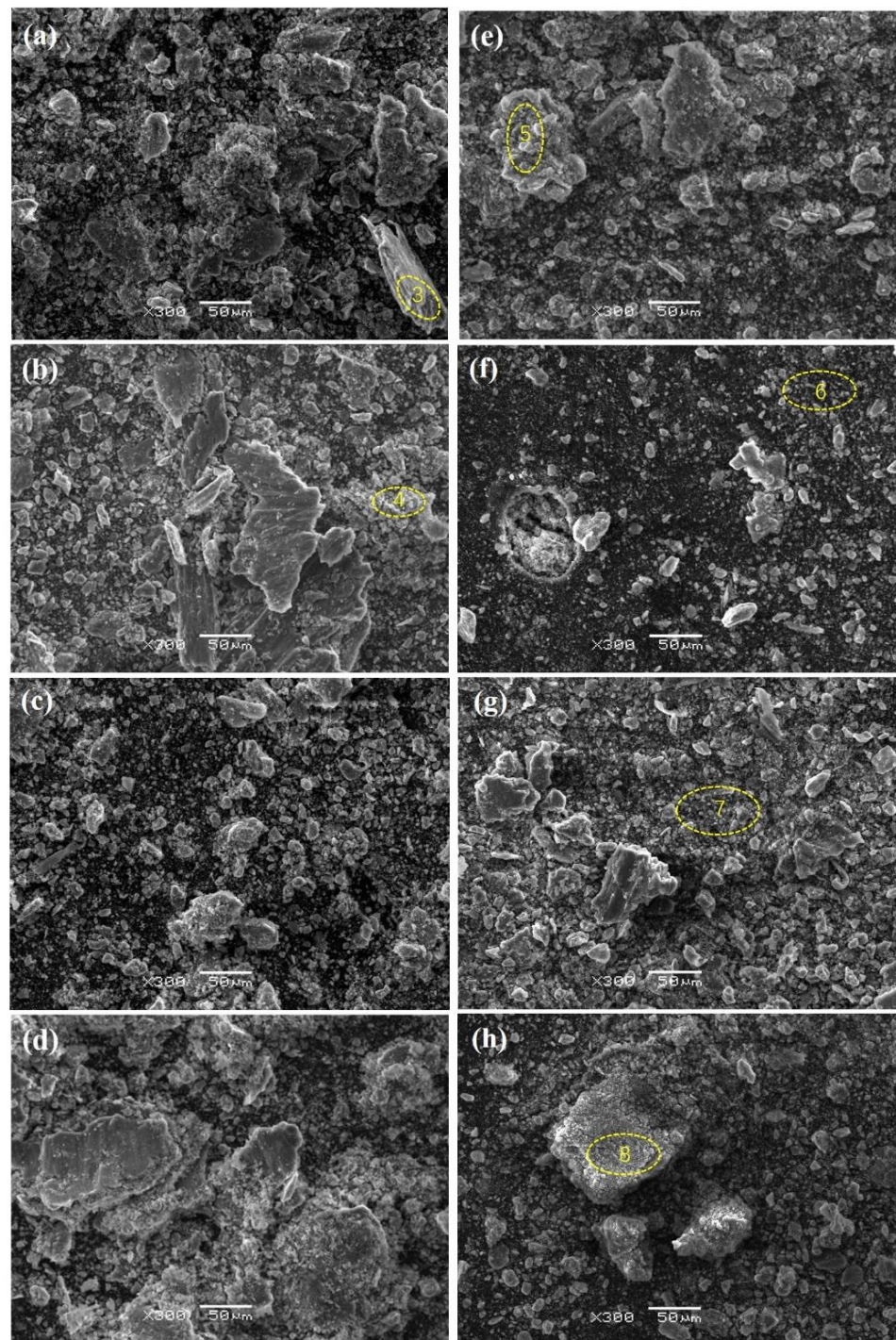


**Figure 9.** SEM images of wear debris of the as-extruded (a–d) and as-aged (e–h) alloys. (a) E-Alloy 0; (b) E-Alloy 1; (c) E-Alloy 2; (d) E-Alloy 3; (e) T5-Alloy 0; (f) T5-Alloy 1; (g) T5-Alloy 2; (h) T5-Alloy 3. The EDS results of yellow circles are shown in Table 2.

The collected wear debris of the alloys is shown in Figure 9, and the compositions of the debris marked in Figure 9 are also listed in Table 2. It can be seen as some large blocks of debris besides numerous tiny debris. They are generated through abrasive wear and/or delamination wear. The composition analysis listed in Table 2 shows that less oxygen is detected in the large block debris (area 3 and area 5), but more oxygen is detected in the tiny debris (area 4 and area 6), which indicates that the tiny debris undergoes more oxidation during dry sliding as a result of the oxidation wear mechanism.

**Table 2.** EDS results of the regions marked in Figure 9.

	Element Content/wt. %					
	Mg	Nd	Gd	Sr	Zn	O
1	Bal.	2.45	3.19	1.39	0.57	9.40
2	Bal.	2.14	2.68	0.97	0.38	16.56
3	Bal.	4.20	0.56	0.81	0.59	12.39
4	Bal.	4.33	2.37	1.35	1.46	9.80
5	Bal.	4.88	1.25	0.8	1.2	8.15
6	Bal.	3.48	1.55	0.71	0.98	13.95
7	Bal.	2.82	3.32	0.28	0.71	10.95
8	Bal.	2.26	4.3	1.14	0.97	11.17

#### 4. Discussion

Studies have shown that both Gd and Nd can refine magnesium alloy grains by inhibiting grain boundary migration [24–27,29]. The solubility of Nd in Mg is much lower than that of Gd in Mg. The redundant Nd would form as the second phase and aggregate at the grain boundaries, which could restrain grain growth. In the present study, as the Gd/Nd ratio increases, the second phase and the aggregated effect at the grain boundaries decrease accordingly, resulting in a decline in microhardness. For the as-extruded alloys, more long elongated grains that did not undergo recrystallization were observed in E-alloy 0, whereas the other as-extruded alloys showed almost complete recrystallization and invisible grain growth. During the aging treatment, some second phases dissolved into the matrix, and more precipitates formed, which impeded grain growth and provided the precipitation-strengthening effect. In addition, most long elongated grains in alloy 0 disappeared due to static recrystallization, and the grains exhibited visible growth in alloys 2 and 3, which is attributed to the increment of the Gd/Nd ratio. Therefore, Nd exhibits more effective grain refining effects as compared with Gd.

It has been reported that when the addition is relatively low, the strengthening of Gd is not as effective as Nd for Mg alloys because of much higher solubility in Mg [24,25,32]. In this study, the total amount of rare earth elements in the four alloys is 4 wt%, and the microhardness of the alloys declines with the increase in Gd/Nd ratio. The precipitates during aging treatment are beneficial to the increase in microhardness.

During the wear experiment, the surface of the magnesium alloy contacts with air and thus forms an oxide film. Owing to the ploughing action of the microscopic bulge of the grinding ball, it would break and fall off, and then the newly exposed surface converted into a new oxide film constantly. The oxide fragments will adhere to the surface of the friction sample and are compacted to form a protective layer to reduce the contact between the friction pair and the alloy surface [33]. Thus, the formation of the oxide film is beneficial to reduce fluctuation of the friction coefficient in the process of friction and wear experiment so that the change of friction coefficient remains stable. Figure 10 is a simple schematic diagram of the wear mechanism of the alloy. The wear behaviors are related to the surface mechanical properties of samples and wear debris generated during sliding [34]. Magnesium alloys tend to react with oxygen. The wear mechanism of most of these alloys is abrasive wear and oxidation wear, similar to Figure 10a. In addition to the oxidation wear and abrasive wear of E-alloy 0 and T5-alloy 1, obvious delamination wear also occurred, as shown in Figure 10b. An oxidation film exists on the surface of alloys, and an oxidation reaction occurs in the friction process due to the action of friction heat, friction pairs, alloy particles, and the oxidation medium in the environment [21,35]. The friction between the friction ball and the hard particles or hard protrusions on the surface of alloys causes the loss of materials, that is, abrasive wear. Each abrasive particle can be considered as continuous debris cut off from the material surface, leaving a furrow on the surface [36], which is shown in Figure 10a. The reason for the delamination wear is that in the process of friction and wear of alloys, partial plastic deformation occurs on the surface when the friction test steel ball is welded to the surface of the magnesium alloy, and further sliding

leads to the spalling of the worn surface and the formation of spalling pits [37], as shown in Figure 10b.

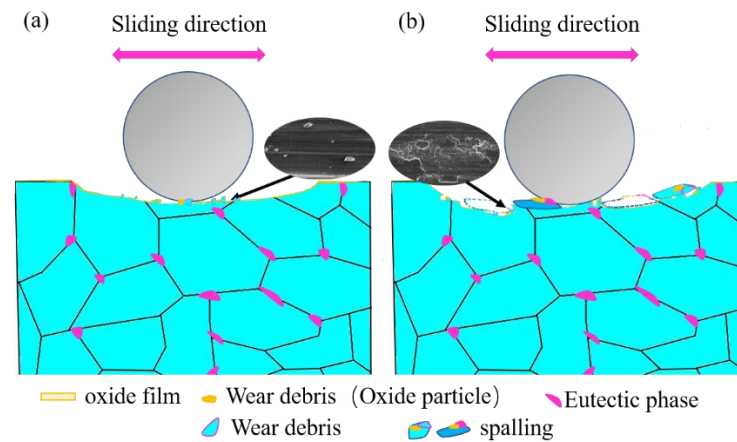


**Figure 10.** Schematic diagram of the wear mechanism of the alloy. (a) abrasive wear; (b) delamination wear.

## 5. Conclusions

The following results were obtained through aging different Gd/Nd ratios extruded alloys of Mg-(4-x)Nd-xGd-0.3Sr-0.2Zn-0.4Zr ( $x = 0, 1, 2, 3$ , Gd/Nd = 0, 1/3, 1, 3) and dry sliding wear before and after aging:

1. With the variation of the Gd/Nd ratio in the alloy, the friction coefficient of the extruded alloy first increases and then decreases, but the friction coefficient of T5 alloys does not change significantly. The friction coefficient of the alloy after T5 treatment is slightly reduced.
2. For the as-aged alloys, the wear rate of the alloy decreases first and then increases with the increase in the Gd/Nd ratio. The alloy with a Gd/Nd ratio of 1/3 after T5 aging treatment has the lowest wear rate and the best wear resistance.
3. The wear mechanisms of the E-alloys and T5-alloys are composed of abrasive wear, oxidation wear, and delamination wear. But the wear mechanisms of T5-Alloy 1 are mainly abrasive wear and oxidation wear, which may be related to its lowest wear rate.

**Author Contributions:** Conceptualization, R.W. (Ruotian Wang) and Y.J.; methodology, R.W. (Rongxiang Wang); software, R.W. (Rongxiang Wang); validation, R.W. (Ruotian Wang), R.W. (Rongxiang Wang) and Y.J.; formal analysis, R.W. (Rongxiang Wang); investigation, R.W. (Ruotian Wang); resources, Y.J.; data curation, Y.J.; writing—original draft preparation, R.W. (Ruotian Wang); writing—review and editing, R.W. (Ruotian Wang) and Y.J.; visualization, Y.J.; supervision, R.W. (Rongxiang Wang); project administration, Y.J.; funding acquisition, Y.J. All authors have read and agreed to the published version of the manuscript.

**Funding:** This research was funded by the Opening Project of Jiangsu Key Laboratory of Advanced Structural Materials and Application Technology, grant number “ASMA202207”.

**Institutional Review Board Statement:** Not applicable.

**Informed Consent Statement:** Not applicable.

**Data Availability Statement:** The data used to support the findings of this study are available from the corresponding author upon request.

**Conflicts of Interest:** Ruotian Wang was employed by the company Yongli Filament & Bristles Co., Limited. The remaining authors declare that the research was conducted in the absence of any commercial or financial relationships that could be construed as a potential conflict of interest.

## References

1. Liu, H.; Huang, H.; Wang, C.; Sun, J.P.; Chen, X.B. Recent advances in LPSO-containing wrought magnesium alloys: Relationships between processing, microstructure, and mechanical properties. *JOM* **2019**, *71*, 3314–3327. [[CrossRef](#)]
2. Song, J.F.; She, J.; Chen, D.L.; Pan, F.S. Latest research advances on magnesium and magnesium alloys worldwide. *J. Magnes. Alloys* **2020**, *8*, 1–41. [[CrossRef](#)]
3. Zhang, X.B.; Ba, Z.X.; Wang, Z.Z.; Wu, Y.J.; Xue, Y.J. Effect of LPSO structure on mechanical properties and corrosion behavior of as-extruded GZ51K magnesium alloy. *Mater. Lett.* **2016**, *163*, 250–253. [[CrossRef](#)]
4. Chen, H.M.; Han, D.; Cui, H.W.; Zhang, L.; Jin, Y.X. Microstructures and properties of As-cast rare earth magnesium alloy with LPSO phase. *Mater. Res. Express* **2019**, *6*, 965a. [[CrossRef](#)]
5. Chen, L.W.; Zhao, Y.H.; Li, M.X.; Li, L.M.; Hou, L.F.; Hou, H. Reinforced AZ91D magnesium alloy with thixomolding process facilitated dispersion of graphene nanoplatelets and enhanced interfacial interactions. *Mat. Sci. Eng. A-Struct.* **2021**, *804*, 140793. [[CrossRef](#)]
6. Ramalingam, V.V.; Ramasamy, P.; Kovukkal, M.D.; Myilsamy, G. Research and development in magnesium alloys for industrial and biomedical applications: A review. *Met. Mater. -Int.* **2020**, *26*, 409–430. [[CrossRef](#)]
7. Han, G.S.; Chen, D.; Chen, G.; Huang, J.H. Development of non-flammable high strength extruded Mg-Al-Ca-Mn alloys with high Ca/Al ratio. *J. Mater. Sci. Technol.* **2018**, *34*, 2063–2068. [[CrossRef](#)]
8. Patel, S.M.; Rao, V.J. Effect of Mn on microstructure, mechanical properties, and corrosion behaviour of Mg-Ni alloys. *Eng. Res. Express* **2022**, *4*, 45035. [[CrossRef](#)]
9. Estrin, Y.; Nene, S.S.; Kashyap, B.P.; Prabhu, N.; Al-Samman, T. New hot rolled Mg-4Li-1Ca alloy: A potential candidate for automotive and biodegradable implant applications. *Mater. Lett.* **2016**, *173*, 252–256. [[CrossRef](#)]
10. Mao, B.; Zhang, X.; Menezes, P.L.; Liao, Y.L. Anisotropic microstructure evolution of an AZ31B magnesium alloy subjected to dry sliding and its effects on friction and wear performance. *Materialia* **2019**, *8*, 100444. [[CrossRef](#)]
11. Liu, Y.; Shao, S.; Xu, C.S.; Yang, X.J.; Lu, D.P. Enhancing wear resistance of Mg-Zn-Gd alloy by cryogenic treatment. *Mater. Lett.* **2012**, *76*, 201–204. [[CrossRef](#)]
12. Cao, L.J.; Wang, Q.D.; Wu, Y.J.; Ye, B. Friction and wear behavior of Mg-11Y-5Gd-2Zn-0.5Zr (wt%) alloy with oil lubricant. *Rare Metals* **2013**, *32*, 453–458. [[CrossRef](#)]
13. Karakulak, E.; Küüker, Y.B. Effect of Si addition on microstructure and wear properties of Mg-Sn as-cast alloys. *J. Magnes. Alloys* **2018**, *6*, 384–389. [[CrossRef](#)]
14. Zafari, A.; Ghasemi, H.M.; Mahmudi, R. Effect of rare earth elements addition on the tribological behavior of AZ91D magnesium alloy at elevated temperatures. *Wear* **2013**, *303*, 98–108. [[CrossRef](#)]
15. Patil, A.; Bontha, S.; Ramesh, M.R. Effect of ECAP on sliding wear behaviour of Mg-Zn-Gd-Zr alloy. *Mater. Today Proc.* **2020**, *20*, 97–102. [[CrossRef](#)]
16. Sravya, T.; Sankaranarayanan, S.; Abdulhakim, A.; Manoj, G. Mechanical properties of magnesium-rare earth alloy systems: A review. *Metals* **2015**, *5*, 1–39.
17. Xie, J.S.; Zhang, J.H.; You, Z.H.; Liu, S.J.; Feng, J. Towards developing Mg alloys with simultaneously improved strength and corrosion resistance via RE alloying. *J. Magnes. Alloys* **2020**, *9*, 41–56. [[CrossRef](#)]
18. Zhang, J.; Zhang, X.B.; Liu, Q.H.; Yang, S.J.; Wang, Z.Z. Effects of load on dry sliding wear behavior of Mg-Gd-Zn-Zr alloys. *J. Mater. Sci. Technol.* **2017**, *33*, 645–651. [[CrossRef](#)]
19. Effects of lanthanum and cerium mixed rare earth metal on abrasion and corrosion resistance of AM60 magnesium alloy. *Rare Metal. Mat. Eng.* **2015**, *44*, 521–526. [[CrossRef](#)]
20. Jiang, J.; Bi, G.L.; Zhao, L.; Li, R.G.; Lian, J.S.; Jiang, Z.H. Dry sliding wear behavior of extruded Mg-Sn-Yb alloy. *J. Rare Earths* **2015**, *33*, 77–85. [[CrossRef](#)]
21. Li, N.; Yan, H. The effects of rare earth Pr and heat treatment on the wear properties of AZ91 alloy. *Crystals* **2018**, *8*, 256. [[CrossRef](#)]
22. Karuppusamy, P.; Lingadurai, K.; Sivananth, V. Effects of T4 and T6 heat treatments on the wear behaviour of WC-reinforced Mg alloy matrix composite. *Trans. Indian Inst. Met.* **2020**, *73*, 521–530. [[CrossRef](#)]
23. Hu, M.L.; Wang, Q.D.; Chen, C.J.; Yin, D.D.; Ding, W.J.; Ji, Z.S. Dry sliding wear behaviour of Mg-10Gd-3Y-0.4Zr alloy. *Mater. Des.* **2012**, *42*, 223–229. [[CrossRef](#)]
24. Zhang, X.B.; Xue, Y.J.; Wang, Z.Z.; He, X.C.; Wang, Q. Microstructure, mechanical and corrosion properties of Mg-(4-x)Nd-xGd-Sr-Zn-Zr biomagnesium alloys. *Acta Metall. Sin.* **2014**, *50*, 979–988.
25. Zhang, X.B.; Sun, W.; Xue, Y.J.; Wang, Z.Z.; Wang, Q. Effect of Gd/Nd ratio on mechanical and biocorrosion properties of as-extruded Mg-Nd-Gd-Sr-Zn-Zr alloys. *Mater. Res. Innov.* **2015**, *19*, S236–S239. [[CrossRef](#)]
26. Azzeddine, H.; Hanna, A.; Dakhouche, A.; Rabahi, L.; Baudin, T. Impact of rare-earth elements on the corrosion performance of binary magnesium alloys. *J. Alloys Compd.* **2020**, *829*, 154569. [[CrossRef](#)]
27. Dinesh, P.; Manivannan, S.; Babu, S.P.K.; Natarajan, S. Effect of Nd on the microstructure and corrosion behaviour of Mg-9Li-3Al magnesium alloy in 3.5 wt.% NaCl solution. *Mater. Today Proc.* **2019**, *15*, 126–131. [[CrossRef](#)]
28. Li, Y.T.; Chen, X.M.; Zeng, X.K.; Liu, M.; Jiang, X.; Leng, Y.X. Hard yet tough and self-lubricating (CuNiTiNbCr)Cx high-entropy nanocomposite films: Effects of carbon content on structure and properties. *J. Mater. Sci. Technol.* **2024**, *173*, 20–30. [[CrossRef](#)]
29. Hu, M.L.; Wang, Q.D.; Ji, Z.S.; Xu, H.Y.; Xin, M.D.; Ma, G.R. Wear behavior of Mg-10Y-4Gd-1.5Zn-0.4Zr alloy. *Trans. Nonferrous Met. Soc. China* **2016**, *26*, 406–413. [[CrossRef](#)]

30. Ramesh, S.; Anne, G.; Nayaka, H.S.; Sahu, S.; Ramesh, M.R. Investigation of dry sliding wear properties of multi-directional forged Mg–Zn alloys. *J. Magnes. Alloys* **2019**, *7*, 444–455. [[CrossRef](#)]
31. Banijamali, S.M.; Palizdar, Y.; Najafi, S.; Sheikhani, A.; Torkamani, H. Effect of Ce addition on the tribological behavior of ZK60 Mg alloy. *Met. Mater. -Int.* **2020**, *27*, 2732–2742. [[CrossRef](#)]
32. Luo, S.F.; Yang, G.Y.; Qin, H.; Xiao, L.; Jie, W.Q. Substitution Effects of Gd with Nd on Microstructures and Mechanical Properties of Mg-10Gd-0.4Zr Alloys. *Adv. Eng. Mater.* **2020**, *22*, 1901576. [[CrossRef](#)]
33. Selvan, S.A.; Ramanathan, S. Dry sliding wear behavior of as-cast ZE41A magnesium alloy. *Mater. Des.* **2010**, *31*, 1930–1936. [[CrossRef](#)]
34. Zhao, P.B.; Zhu, J.P.; Yang, K.J.; Li, M.L.; Shao, G.; Lu, H.X.; Ma, Z.; Wang, H.L.; He, J.L. Outstanding wear resistance of plasma sprayed high-entropy monoboride composite coating by inducing phase structural cooperative mechanism. *Appl. Surf. Sci.* **2023**, *616*, 156516. [[CrossRef](#)]
35. Xu, J.; Wang, X.W.; Zhu, X.C.; Shirooyeh, M.; Langdon, T.G. Dry sliding wear of an AZ31 magnesium alloy processed by equal-channel angular pressing. *J. Mater. Sci.* **2013**, *48*, 4117–4127. [[CrossRef](#)]
36. Seenuvasaperumal, P.; Doi, K.; Basha, D.A.; Singh, A.; Elayaperumal, A.; Tsuchiya, K. Wear behavior of HPT processed UFG AZ31B magnesium alloy. *Mater. Lett.* **2018**, *227*, 194–198. [[CrossRef](#)]
37. Ajith Kumar, K.K.; Pillai, U.T.S.; Pai, B.C.; Chakraborty, M. Dry sliding wear behaviour of Mg-Si alloys. *Wear* **2013**, *303*, 56–64. [[CrossRef](#)]

**Disclaimer/Publisher’s Note:** The statements, opinions and data contained in all publications are solely those of the individual author(s) and contributor(s) and not of MDPI and/or the editor(s). MDPI and/or the editor(s) disclaim responsibility for any injury to people or property resulting from any ideas, methods, instructions or products referred to in the content.